COLLOQUIA: LaThuile10

Recent charmonium results from CLEO-c

C. M. TARBERT for the CLEO COLLABORATION

Department of Physics, Indiana University - Bloomington, Indiana 47405, USA

Summary. — In this paper I present three of the latest results in charmonium from the CLEO-c experiment.

PACS `13.20.Fc` – Decays of charmed mesons.
PACS `13.40.Em` – Electric and magnetic moments.

1. – Introduction

The CLEO Collaboration was formed in 1975 initially with the goal of studying e^+e^- collisions between $\sqrt{s} = 8$ and $16\,\text{GeV}$ at the newly proposed Cornell Electron Storage Ring (CESR). Over the last 35 years, CLEO have operated a series of experiments at CESR using bottomonium, B-decays, charmonium and D-decays as laboratories for QCD studies. The latest, and final, incarnation of the CLEO detector system was dubbed CLEO-c, with the suffix indicating its intended purpose; detailed studies of charm physics. Large data sets were acquired both above and below open charm threshold and here, I will present three of the latest results obtained in charmonium. The goals of these analyses are varied and give an indication of the scope of physics accessible in this region of the charmonium spectrum. The first result is the outcome of a search for higher-order multipole transitions in charmonium radiative transitions [1]. These transitions provide access to one of the fundamental properties of the charm quark: its anomalous magnetic moment. The second result is a measure of the relative rate of hadronic and radiative decays of the $\psi(2S)$, a ratio which is sensitive to the strong coupling constant [2]. Finally, I will present the latest precision measurements of hadronic χ_{cJ} branching fractions to $p\bar{p}\pi^0$, $p\bar{p}\eta$ and $p\bar{p}\omega$ [3] which have applications to studies of nucleon-nucleon interactions as well as $p\bar{p}$-annihilation experiments.

2. – CLEO-c experiment and data sets

CLEO-c [4] is a hermetic and symmetric detector covering 93% of the $4\pi\,\text{sr}$ of solid angle. It features a $1\,\text{T}$ superconducting solenoid which houses drift chambers for tracking and particle identification and a ring imaging Cerenkov (RICH) system to further

differentiate between charged particle species. Also housed within the solenoid volume is an electromagnetic calorimeter composed of 7784 CsI(Tl) crystals. The photon energy resolution is 2.2% at $1\,\text{GeV}$ and 5% at $100\,\text{MeV}$ and the momentum resolution achieved using the drift chambers is typically 0.6% at $1\,\text{GeV}/c$.

The data sets taken with the CLEO-c configuration include $600\,\text{pb}^{-1}$ at $\sqrt{s} = 4.170\,\text{GeV}/c^2$ and $818\,\text{pb}^{-1}$ at $\sqrt{s} = 3.770\,\text{GeV}/c^2$. At centre-of-mass energies above the threshold for $D\bar{D}$ production, these data are designed for open charm studies. The results presented here, however, utilise a $54\,\text{pb}^{-1}$ data set taken at $\sqrt{s} = 3.686\,\text{GeV}/c^2$ equivalent to the production of 27×10^6 $\psi(2S)$ mesons. Since it is below $D\bar{D}$-production threshold, the $\psi(2S)$ cannot decay to open charm as favoured according to the Okubo-Zweig-Iizukawere (OZI) rule. Instead, the $\psi(2S)$ frequently transitions to a lower mass charmonium state with a branching fraction of 59% for $\psi(2S) \rightarrow J/\psi X$ and around 9% for each of the radiative transitions $\psi(2S) \rightarrow \gamma\chi_{cJ}$ where $J = 0, 1$ and 2. As a result, this data set provides not only access to the $\psi(2S)$ but to the entire charmonium spectrum below $D\bar{D}$ threshold.

3. – Higher-order multipole transitions in charmonium radiative transitions

The radiative transitions

$$(1) \qquad \psi' \rightarrow \gamma'\chi_{cJ}, \qquad \chi_{cJ} \rightarrow \gamma J/\psi,$$

where $J = 0, 1, 2$ and $\psi' \equiv \psi(2S)$, are dominated by processes where $E1$ photons are emitted. However, angular momentum and parity conservation do not rule out the possibility of higher-order multipole transitions. When the decay proceeds through the χ_{c0}, only an $E1$ transition is allowed. However, when the decay involves the χ_{c1} both $E1$ and $M2$ transitions are allowed and in the χ_{c2} case, $E1$, $M2$ and $E3$ transitions are permitted although the single quark radiation hypothesis predicts that the $E3$ amplitude should be zero in the absence of $\psi(2S)$ S-D-mixing and χ_{cJ} P-F-mixing. One can picture electric transitions in the $c\bar{c}$ bound state as arising due to interactions between the charge of one quark and the electric field of the other. Similarly, magnetic transitions originate from the magnetic moment of one quark interacting with the magnetic field of the other. The presence of higher-order magnetic multipole radiative transitions can therefore act as a probe of the c-quark magnetic moment. The first attempt to measure $M2$ amplitudes in charmonium transitions was made shortly after the discovery of the J/ψ. That measurement and subsequent results are in some disagreement with the theoretical predictions [5], and it is the aim of this analysis to apply the large statistics CLEO-c data set to the problem.

If the $\psi(1S, 2S)$ are pure S states and the χ_{cJ}'s are pure P states, then one can assume the following non-relativistic interaction Hamiltonian for photon emission from a $+2/3$ charged quark:

$$(2) \qquad H = -\frac{e_c}{2m_c}\left(\mathbf{A}^* \cdot \mathbf{p} + \mathbf{p} \cdot \mathbf{A}^*\right) - \mu\sigma \cdot \mathbf{H}^*,$$

where $\mu \equiv (e_c/2m_c)(1+\kappa_c)$ and m_c, e_c and κ_c are the mass, electric charge and anomalous magnetic moment of the c-quark. The electric and magnetic fields of the emitted photon are represented by $\mathbf{A}^*$ and $\mathbf{H}^*$, respectively. Expanding (2) in powers of E_γ/m_c, the

normalised magnetic quadrupole amplitudes can be expressed (to first order) as

$$
(3) \qquad a_2^{J=1} \equiv \frac{M2}{\sqrt{E1^2 + M2^2}} = -\frac{E_\gamma}{4m_c}\left(1 + \kappa_c\right),
$$

$$
a_2^{J=2} \equiv \frac{M2}{\sqrt{E1^2 + M2^2 + E3^2}} = -\frac{3}{\sqrt{5}}\frac{E_\gamma}{4m_c}\left(1 + \kappa_c\right),
$$

$$
b_2^{J=1} \equiv \frac{M2}{\sqrt{E1^2 + M2^2}} = -\frac{E_{\gamma'}}{4m_c}\left(1 + \kappa_c\right),
$$

$$
b_2^{J=2} \equiv \frac{M2}{\sqrt{E1^2 + M2^2 + E3^2}} = -\frac{3}{\sqrt{5}}\frac{E_{\gamma'}}{4m_c}\left(1 + \kappa_c\right).
$$

The letter b is used to denote amplitudes before the χ_{cJ}, *i.e.* $\psi' \to \gamma'\chi_{cJ}$ and a denotes amplitudes after the χ_{cJ}, *i.e.* $\chi_{cJ} \to \gamma J/\psi$. The subscript indicates the multipole order and the superscript gives the angular momentum of the χ_{cJ}. Using (3) and choosing values for κ_c and m_c, one can obtain predictions for the magnetic quadrupole amplitudes. It is also important to note that the ratios of these amplitudes are independent of κ_c and m_c to first order in E_γ/m_c.

Events are fully reconstructed in the CLEO-c apparatus in the decay mode $\psi' \to \gamma'\chi_{cJ}$; $\chi_{cJ} \to \gamma J/\psi$; $J/\psi \to l^+l^-$, where l is an electron or muon. To extract $a_2^{J=1}$, $b_2^{J=1}$ and $a_2^{J=2}$, $b_2^{J=2}$ from the data, the joint angular distribution of the two radiated photons, W, is first constructed in the helicity formalism:

$$
(4) \qquad W\left(\cos\theta', \phi', \cos\theta_{\gamma\gamma'}, \cos\theta, \phi\right)
$$

$$
\propto \sum \rho^{(\mu'-\nu',\mu'-\bar{\nu}')}(\theta', \phi') B_{|\nu'|} B_{|\bar{\nu}'|} d^{J_\chi}_{-\nu'\nu}(\theta_{\gamma\gamma'})
$$

$$
\times d^{J_\chi}_{-\bar{\nu}'\bar{\nu}}(\theta_{\gamma\gamma'}) A_{|\nu|} A_{|\bar{\nu}|} \rho^{*(\nu-\mu,\nu-\bar{\mu})}(\theta, \phi),
$$

where μ', ν', μ and ν are the helicities of the γ', χ_{cJ}, γ and J/ψ, respectively. The angles θ' and ϕ' are defined in the ψ' rest frame and are sensitive to the polarisation of the ψ', while θ and ϕ are defined in the J/ψ frame and are sensitive to the polarisation of the J/ψ. The final angle needed to completely define the decay, $\theta_{\gamma\gamma'}$, gives the relative orientation of the ψ'- and J/ψ-frames. The helicity amplitudes A and B are extracted from the data via a five-dimensional unbinned extended maximum likelihood fit and are related to the normalised magnetic dipole amplitudes, a_2^J, b_2^J via Clebsch-Gordon coefficients.

Initially, two-parameter fits to the χ_{c1} and χ_{c2} data were performed to extract $a_2^{J_\chi=1}$, $b_2^{J_\chi=1}$ and $a_2^{J_\chi=2}$, $b_2^{J_\chi=2}$, respectively. The results from these fits are shown in fig. 1(A) where the data are overlayed with projections of the fitted PDF. The projections were generated by weighting MC samples containing 4.5×10^6 phase space events with W. From inspection of fig. 1(A), it is clear that the data is better described by the fitted PDF containing non-zero $M2$ amplitudes and in fact the pure $E1$ amplitude is inconsistent with the data at the 11σ and 6σ level for the χ_{c1} and χ_{c2} cases, respectively. These fits were repeated, fixing the ratio of $a_2^{J_\chi=1}/b_2^{J_\chi=1}$ and $a_2^{J_\chi=2}/b_2^{J_\chi=2}$; the results from these one-parameter fits were consistent with the initial two-parameter fits. In the χ_{c2} data, there is also potentially an electric octupole component to the decay. An iteration of fits was performed introducing an $E3$ amplitude and allowing it to float in the fit. Again, the fits were repeated, fixing the ratios of the $a_3^{J_\chi=2}/b_3^{J_\chi=2}$. In all cases, there is at least 6σ evidence for non-zero $M2$ amplitudes.
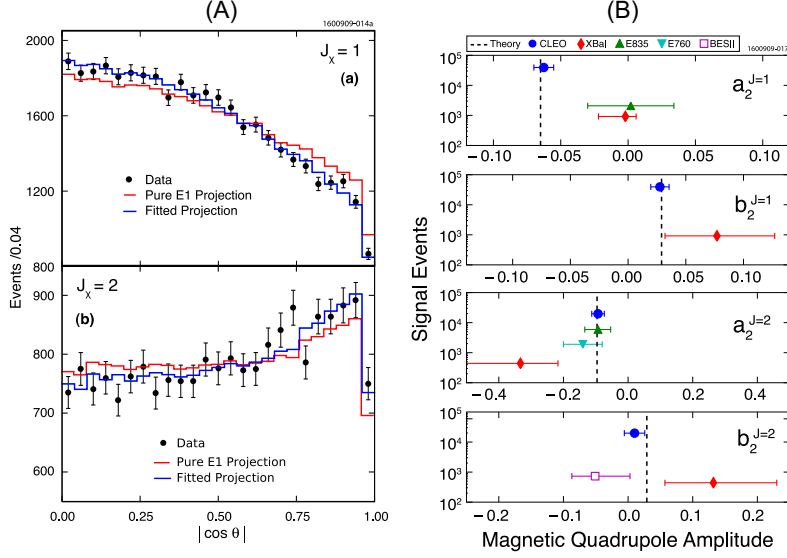
Fig. 1. – Results of the unbinned maximum likelihood fit to extract the normalised magnetic quadrupole amplitudes. (A) Points are data. Red line: projection of W using only a pure $E1$ amplitude for the χ_{c1} data (a) and the χ_{c2} (b). Blue line: projection of W using the fitted non-zero $M2$ amplitudes. (B) Results from this analysis are solid circles, Crystal Ball results are diamonds, the E760 and E835 results [5] are triangles. The line is the theoretical value calculated using (3) and $\kappa_c = 0$, $m_c = 1.5\,\text{GeV}/c^2$.

Figure 1(B) shows a comparison with previous experimental results and highlights the greatly increased statistics available to the current measurement. A comparison with a theoretical calculation performed using (3) and assuming $\kappa_c = 0$ and $m_c = 1.5\,\text{GeV}/c^2$ is also presented and shows the current result to be in excellent agreement with theory. Furthermore, ratios of the normalised $M2$ amplitudes, which are independent of κ_c and m_c, were also found to be in consistent with the values predicted by eq. (3).

4. – Inclusive ψ' decays

The OZI-favoured decay channels to open charm are not available to the $\psi(2S)$ and instead, it must decay via $c\bar{c}$-annihilation. The next lowest-order decay processes are annihilation to three gluons ($c\bar{c} \to ggg$), to two gluons and a photon ($c\bar{c} \to \gamma gg$) or to a virtual photon ($c\bar{c} \to \gamma* \to q\bar{q}$). Given that $\Gamma(\psi(2S) \to \gamma gg) \propto \alpha_s^2 \alpha_{em}$ and $\Gamma(\psi(2S) \to ggg) \propto \alpha_s^3$ a rough expectation for the ratio $R_\gamma(\psi(2S))$ can be obtained:

$$(5) \qquad R_\gamma\left(\psi\left(2S\right)\right) = \frac{\Gamma\left(\psi(2S) \to \gamma gg\right)}{\Gamma\left(\psi(2S) \to ggg\right)} \propto q_c^2 \frac{\alpha_{em}}{\alpha_s}\ .$$

There are no previous measurements of $R_\gamma(\psi(2S))$, however, a new measurement of $R_\gamma(J/\psi)$ was recently reported by the CLEO Collaboration [6]. Prior to that, a survey of R_γ in bottomonium was made [7] and these results are summarised in table I. Examining table I, one would naively expect to see a similar trend in charmonium, that is, $R_\gamma(\psi(2S)) \sim R_\gamma(J/\psi)$.

TABLE I. – *Summary of latest R_γ measurements [2,6,7]. Errors are statistical then systematic.*

$R_\gamma(J/\psi)$	$(0.137 \pm 0.001 \pm 0.016)$
$R_\gamma(\psi(2S))$	$(0.097 \pm 0.002 \pm 0.026)$
$R_\gamma(\Upsilon(1S))$	$(0.027 \pm 0.001 \pm 0.003)$
$R_\gamma(\Upsilon(2S))$	$(0.032 \pm 0.001 \pm 0.005)$
$R_\gamma(\Upsilon(3S))$	$(0.027 \pm 0.001 \pm 0.005)$

The ratio R_γ can be expressed as $R_\gamma = N_{\gamma gg}/(N_{ggg}\epsilon_{\gamma gg})$, where $N_{\gamma gg}$ is the number of direct photon decays observed in the data, N_{ggg}, the number of three gluon decays, and $\epsilon_{\gamma gg}$ is the direct photon finding efficiency. The denominator of this expression was previously measured by CLEO [8]. The experimental approach to obtain $R_\gamma(\psi(2S))$ is then to measure the inclusive photon spectrum from $\psi(2S) \to \gamma X$, and subtract off everything that does not arise due to $\psi(2S) \to \gamma gg$. An analysis of Monte Carlo samples (fig. 2(A)) gives an indication of the relative strength of backgrounds competing with the $\psi(2S) \to \gamma gg$ signal to contribute to the observed photon spectrum. The background is dominated by the two photon decays of π^0 and η mesons as well as radiative decays of the J/ψ, which are produced copiously via the hadronic transitions $\psi(2S) \to J/\psi X$. The J/ψ direct photon decay spectrum in this data set has been previously measured [6] and can be subtracted off directly. Two different techniques are then used to account for the $(\pi^0, \eta) \to \gamma\gamma$ background.

In the first method, an exponential function is fitted to the observed photon spectrum in a region where $\pi^0 \to \gamma\gamma$ processes dominate; $0.27 < z_\gamma < 0.32$. The distribution is then extrapolated to higher photon energies and subtracted off the observed spectrum. An alternative background subtraction technique exploits the isospin relationship between the π^0, π^+ and π^- and the resulting expected similarities in kinematics. The four-momenta of charged pions found in the data are used to generate an estimated background spectrum by treating them as neutral pions, and forcing them to decay to two back-to-back photons in the pion rest frame. After applying the photon-finding efficiency extracted from Monte Carlo simulations, the resulting "pseudophoton" energy spectrum is normalised according to isospin constraints and subtracted from the observed photon spectrum. This pseudophoton approach has been used in previous analyses and is described in more detail in ref. [6]. The photon spectrum after each of these subtractions has been applied is shown in fig. 2(B). Below $z_\gamma \sim 0.4$, the distribution is dominated by soft photons from radiative transitions to lower mass $c\bar{c}$ states; the peak around $z_\gamma \sim 0.34$ is from transitions to the η_c. Two values of $N_{\gamma gg}$ are initially obtained by integrating the exponential-subtracted and pseudophoton-subtracted distributions above $z_\gamma \sim 0.4$ and extrapolating to $z_\gamma \to 0$. Since the background elimination techniques give rise to the possibility of over- or under-subtraction, a cross check is performed exploiting the prominent $\psi(2S) \to \gamma\eta_c$ line. First, a distribution is obtained by averaging the exponential- and pseudophoton-subtracted spectra. A fit is performed in the interval $0.32 < z_\gamma < 0.38$ to obtain the number of $\psi(2S) \to \gamma\eta_c$ events which can then be used to normalise the distribution using the known $\psi(2S) \to \gamma\eta_c$ branching fraction. By integrating and normalising the averaged distribution, a third value for $R_\gamma(\psi(2S))$ is obtained. A weighted averaged of all three values of R_γ is made and this is included in table I. As fig. 2(A) demonstrates, the signal-to-noise ratio in the direct photon spectrum is small. As a result, fluctuations in the estimated background have a large effect on the extracted value
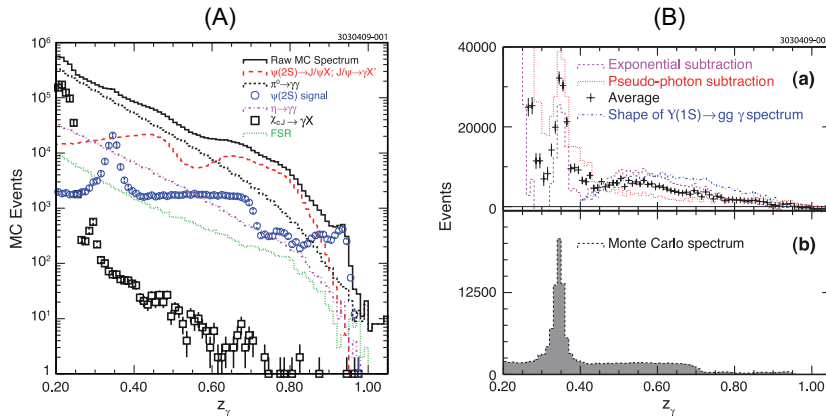
Fig. 2. – Figures from inclusive $\psi(2S)$ radiative decays analyis. $z_\gamma = E_\gamma / E_{\text{beam}}$. (A) Relative contribution of backgrounds to the inclusive $\psi(2S)$ direct photon decay spectrum from analysis of Monte Carlo samples. (B) Inclusive $\psi(2S)$ decay photon spectrum in data after background subtraction (a). $\psi(2S) \to \gamma gg$ direct photon spectrum from analysis of Monte Carlo samples (b).

of R_γ. Investigations of the sensitivity of R_γ to the background scale have led to the assignment of a systematic error due to uncertainties in the background level of 27% and this is by far the dominating systematic.

Since $\Gamma(\psi(3770) \to \gamma gg)$ is immeasurably small, this completes the set of R_γ for the ψ $J^{PC} = 1^{--}$ states. Although the difference between $R_\gamma(J/\psi)$ and $R_\gamma(\psi(2S))$ is considerably larger than the corresponding differences in the Υ results, the large systematic error on $R_\gamma(\psi(2S))$ means the difference is only equivalent to $\sim 1\sigma$ deviation. However, it is possible that this large systematic is masking another example of unexpected $\psi(2S)$ to J/ψ partial widths ratios, *e.g.*, the "$\rho\pi$ puzzle" [9].

5. – Exclusive χ_{cJ} decays

The recent theoretical work of Barnes *et al.* [10, 11] emphasises the importance of studying processes such as $\Psi \to p\bar{p}m$ where Ψ is any $c\bar{c}$ state and m is a light meson. Their work allows measured $\Psi \to p\bar{p}m$ partial widths to be used to estimate the production cross sections $\sigma(p\bar{p} \to \Psi m)$, circumventing the calculation of some of the complicated underlying QCD processes. These theoretical studies are particularly important for the upcoming PANDA experiment which will use associated charmonium production in $p\bar{p}$ annihilation ($p\bar{p} \to \Psi m$) as a tool in its search for exotic hybrid mesons in the charm sector. Furthermore, the techniques developed in refs. [10] were extended in ref. [11] to allow for the prediction of $\Psi \to p\bar{p}m$ partial widths. In their meson emission model, the authors assume the sequential decay $\Psi \to p\bar{p} \to p\bar{p}m$ and they estimate $\Gamma(\Psi \to p\bar{p}m)$ using the measured $\Psi \to p\bar{p}$ widths and well-known $p\bar{p}m$ coupling constants. If this sequential decay mechanism is in fact the dominant means by which $\Psi \to p\bar{p}m$ decays proceed, then the branching fractions to $p\bar{p}m$ final states would provide a means of extracting other meson-nucleon coupling constants [11]. The first measurements of $\mathcal{B}(\chi_{cJ} \to p\bar{p}\pi^0)$ and $\mathcal{B}(\chi_{cJ} \to p\bar{p}\eta)$ were reported by CLEO in 2007 [12]. Here, we exploit a factor of 10 increase in statistics to improve on those measurements. Furthermore, we report the first measurement of $\mathcal{B}(\chi_{cJ} \to p\bar{p}\omega)$.

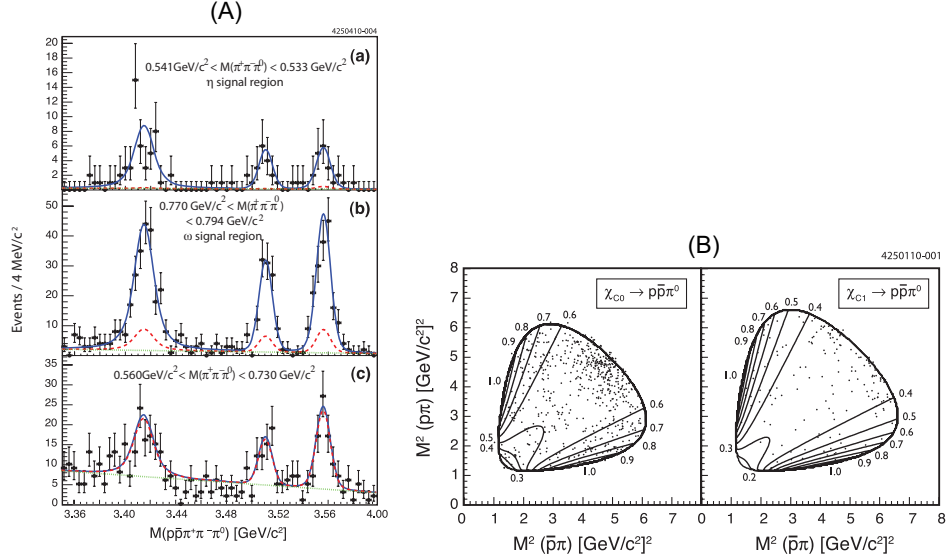Fig. 3. – Figures from analysis of exclusive χ_{cJ} decays. (A) Projections of best fit to $M(p\bar{p}\pi^+\pi^-\pi^0)$, $M(\pi^+\pi^-\pi^0)$ for three regions of $M(\pi^+\pi^-\pi^0)$. Markers are data. Solid line: total fitted PDF. Dashed line: non-resonant background component of fitted PDF. Dotted line: linear background component of fit. (B) Dalitz plot for $\chi_{cJ} \to p\bar{p}\pi^0$. Points are data, contours are from the meson emission model of ref. [11].

In this analysis, two final states are fully reconstructed in the CLEO-c apparatus: $\psi(2S) \to \gamma\chi_{cJ}$; $\chi_{cJ} \to p\bar{p}\gamma\gamma$ and $\psi(2S) \to \gamma\chi_{cJ}$; $\chi_{cJ} \to p\bar{p}\pi^+\pi^-\pi^0$. As well as giving access to the $\chi_{cJ} \to p\bar{p}\omega$ channel, this allows the $\chi_{cJ} \to p\bar{p}\eta$ channel to be reconstructed in two separate decay modes. The desired branching fractions are calculated according to

$$(6) \qquad \mathcal{B}\left(\chi_{cJ} \to p\bar{p}m\right) = \frac{N_m}{\epsilon_m N_{\psi(2S)} \mathcal{B}\left(\psi(2S) \to \gamma\chi_{cJ}\right) \mathcal{B}\left(m \to Y\right)} \, .$$

$N_{\psi(2S)}$ is the number of $\psi(2S)$ present in the data and ϵ_m is the signal efficiency evaluated via analysis of MC samples. The branching fractions $\mathcal{B}(\psi(2S) \to \gamma\chi_{cJ})$ are those measured by CLEO [13] and values for $\mathcal{B}(m \to Y)$, where Y represents either $\gamma\gamma$ or $\pi^+\pi^-\pi^0$, are taken from the 2008 Particle Data Group report. The signal yield, N_m, is extracted from the data using slightly different techniques for the $p\bar{p}\gamma\gamma$ and $p\bar{p}\pi^+\pi^-\pi^0$ final states. In the first case, the strength is extracted via a one-dimensional unbinned extended maximum likelihood fit to the candidate χ_{cJ} mass spectrum. There is a large non-resonant background in the $p\bar{p}\pi^+\pi^-\pi^0$ channel, making it impossible to reliably extract the signal strengths from fits to $M(p\bar{p}\pi^+\pi^-\pi^0)$ alone. Instead, a two-dimensional unbinned extended maximum likelihood fit is performed in $M(p\bar{p}\pi^+\pi^-\pi^0)$ and $M(\pi^+\pi^-\pi^0)$ and the $p\bar{p}\eta[\pi^+\pi^-\pi^0]$ and $p\bar{p}\omega$ yields are extracted simultaneously. Fitting in both variables provides sensitivity to the non-resonant shape over a wide range of $M(\pi^+\pi^-\pi^0)$ and allows the contribution in the η and ω signal regions to be pinned down.

The results of the fit to the $p\bar{p}\pi^+\pi^-\pi^0$ final state are shown in fig. 3(A) and the extracted branching fractions for all channels are listed in table II. The meson emission model predictions for the two branching fractions $\mathcal{B}(\chi_{c0} \to p\bar{p}\pi^0)_{\text{theory}} = 2.5 \times 10^{-4}$ and

TABLE II. – *Final $\chi_{cJ} \to p\bar{p}m$ branching fractions. Uncertainties are statistical then systematic, then a separate systematic error due to the uncertainty in the $\psi(2S) \to \gamma\chi_{cJ}$ branching fractions.*

$(\times 10^{-4})$	χ_{c0}	χ_{c1}	χ_{c2}
$p\bar{p}\pi^0$	$(7.76 \pm 0.37 \pm 0.51 \pm 0.39)$	$(1.75 \pm 0.16 \pm 0.13 \pm 0.11)$	$(4.83 \pm 0.25 \pm 0.35 \pm 0.31)$
$p\bar{p}\eta$	$(3.73 \pm 0.38 \pm 0.28 \pm 0.19)$	$(1.56 \pm 0.22 \pm 0.14 \pm 0.10)$	$(1.76 \pm 0.23 \pm 0.14 \pm 0.11)$
$p\bar{p}\omega$	$(5.57 \pm 0.48 \pm 0.50 \pm 0.28)$	$(2.28 \pm 0.28 \pm 0.20 \pm 0.14)$	$(3.68 \pm 0.35 \pm 0.31 \pm 0.24)$

$\mathcal{B}(\chi_{c1} \to p\bar{p}\pi^0)_{\text{theory}} = 0.2 \times 10^{-4}$ [11] are well below our observed branching fractions, by factors of about 3 and 10, respectively. This suggests that meson emission, as described by this model, is not the dominant decay mechanism. This can be further demonstrated by comparing the theoretical Dalitz plot event densities calculated in ref. [11] with our data; this comparison is shown in fig. 3(B). The meson emission model predicts strength in regions of low $p\pi^0$ and $\bar{p}\pi^0$ invariant mass, whereas the data show a clear enhancement at low $p\bar{p}$ invariant mass.

* * *

REFERENCES

[1] ARTUSO M. *et al.*, *Phys. Rev. D*, **80** (2009) 112003.
[2] LIBBY J. *et al.*, *Phys. Rev. D*, **80** (2009) 112003.
[3] ONYISI P. *et al.*, LEPP Report No. CLNS 10/2064 (2010).
[4] ARTUSO M. *et al.*, *Nucl. Instrum. Methods A*, **554** (2005) 147; PETERSON D. *et al.*, *Nucl. Instrum. Methods A*, **478** (2002) 142; BRIERE R. A. *et al.* (CESR-C AND CLEO-C TASKFORCES, CLEO-C COLLABORATION, CORNELL UNIVERSITY), LEPP Report No. CLNS 01/1742 (2001) unpublished.
[5] OREGLIA, M *et al.* (CRYSTAL BALL COLLABORATION), *Phys. Rev. D*, **79** (1982) 252259; ARMSTRONG T. *et al.* (E760 COLLABORATION), *Phys. Rev. D*, **48** (1993) 3037; ABILIKIM M. *et al.* (BES COLLABORATION), *Phys. Rev. D*, **70** (2004) 092004.
[6] BESSON D. *et al.*, *Phys. Rev. D*, **78** (2008) 032012.
[7] BESSON D. *et al.*, *Phys. Rev. D*, **74** (2006) 012003.
[8] BESSON D. *et al.*, *Phys. Rev. D*, **78** (2008) 1011102.
[9] GU Y. *et al.*, *Phys. Rev. D*, **63** (2001) 114019.
[10] LUNDBORD A. *et al.*, *Phys. Rev. D*, **73** (2006) 096003; BARNES T. *et al.*, *Phys. Rev. D*, **75** (2007) 054018; **77** (2008) 056001.
[11] BARNES T. *et al.*, *Phys. Rev. D*, **81** (2010) 034025.
[12] ATHAR S. B. *et al.*, *Phys. Rev. D*, **75** (2007) 032002.
[13] ATHAR S. B. *et al.*, *Phys. Rev. D*, **70** (2004) 112002.